Enhanced yellow fluorescent protein photoconversion to a cyan fluorescent protein-like species is sensitive to thermal and diffusion conditions

Merete K. Raarup
Aarhus University
Stereology and Electron Microscopy Research Laboratory
Histoinformatics and MIND Centres
Ole Worms Allé 1185
DK-8000 Aarhus C.
Denmark

Anja W. Fjorback
Aarhus University
Stereology and Electron Microscopy Research Laboratory
Histoinformatics and MIND Centres
Ole Worms Allé 1185
DK-8000 Aarhus C.
Denmark
    and
Aarhus University Hospital
Centre for Psychiatric Research
Skovagervej 2
DK-8240 Risskov
Denmark

Stig M. R. Jensen
Aarhus University
Department of Molecular Biology
C.F. Møllers Allé 1130
DK-8000 Aarhus C.
Denmark

Heidi K. Müller
Aarhus University Hospital
Centre for Psychiatric Research
Skovagervej 2
DK-8240 Risskov
Denmark

Maj M. Kjærgaard
Stereology and Electron Microscopy Research Laboratory
Histoinformatics and MIND Centres
Ole Worms Allé 1185
DK-8000 Aarhus C.
Denmark

Hanne Poulsen
Aarhus University
Department of Molecular Biology
Gustav Wieds Vej 10 C
DK-8000 Aarhus C.
Denmark

Ove Wiborg
Aarhus University Hospital
Centre for Psychiatric Research
Skovagervej 2
DK-8240 Risskov
Denmark

Jens R. Nyengaard
Stereology and Electron Microscopy Research Laboratory
Histoinformatics and MIND Centres
Ole Worms Allé 1185
DK-8000 Aarhus C.
Denmark

Abstract. Ongoing research efforts into fluorescent proteins continuously generates new mutation variants, some of which can become photoactivated or photoconverted to a red-shifted color upon intense UV or blue light illumination. We report a built-in propensity for enhanced yellow fluorescent protein (EYFP) to undergo irreversible photoconversion into a cyan fluorescent protein (CFP)–like species upon green-light illumination. The photoconversion is thermally activated, happens mainly in fixed, nonsealed cell samples, and may result in a very bright and relatively photostable CFP-like species. The photoconversion efficiency depends on the sample diffusivity and is much increased in dehydrated, oxygenated samples. Given the large variations in conversion efficiency observed among samples as well as within a sample, photoconversion cannot be appropriately accounted for in the analysis of acceptor photobleaching fluorescence resonance energy transfer (pbFRET) images and should rather be completely avoided. Thus, samples should always be checked and discarded if photoconversion is observed. © *2009 Society of Photo-Optical Instrumentation Engineers.* [DOI: 10.1117/1.3103338]

1 Introduction

Fluorescent proteins, which can become activated or change color upon UV or visible-light illumination, have recently attracted much interest due to the advantages of such probes in quantitative fluorescence microscopy. Furthermore, they have the potential to shed new light on different photophysical mechanisms taking place among the members of the fluorescent protein color palette.[1] Increasing the understanding of these mechanisms is important in defining their limits of use in various fluorescence assays as well as in the development

Address all correspondence to: Merete K. Raarup, Stereology and Electron Microscopy Research Laboratory, Aarhus University, Ole Worms Allé 1185, DK-8000 Aarhus C., Denmark. Tel. +45 8942 2945; Fax +45 8942 2952; E-mail: raarup@ki.au.dk.

and optimization of new fluorescent markers with specialized properties. For example, in relation to photobleaching fluorescence resonance energy transfer (pbFRET) microscopy, artifacts originating from unexpected photophysical properties can lead to false positive detection of protein-protein interactions. This has been encountered in two studies involving enhanced yellow fluorescent protein (EYFP) as an acceptor, in which a cyan fluorescent protein (CFP)–like signal originating from EYFP was detected upon EYFP photobleaching with green light illumination.[2,3] Interestingly, two other research groups have reported not to observe this EYFP photoconversion.[4] These apparently conflicting results, together with different experimental conditions reported with the studies, prompted us to investigate in detail the conditions under which EYFP might undergo photoconversion. Live and fixed human embryonic kidney 293 (HEK 293) cell samples transfected with EYFP or Venus alone or with EYFP attached to different protein partners [EYFP–serotonin transporter (EYFP-SERT), EYFP–dopamine transporter (EYFP-DAT), adenosine deaminase acting on RNA–EYFP (ADAR2-EYFP)] were examined under a range of experimental conditions using confocal as well as wide-field bleaching illumination. From these studies, we have tracked down some experimental conditions for which EYFP photoconversion is most likely to occur.

2 Materials and Methods

2.1 Plasmids

The EYFP-SERT vector was a generous gift from Dr. H. H. Sitte, University of Vienna, Austria. The Venus vector was kindly provided by Dr. A. Miyawaki, RIKEN Institute of Physical and Chemical Research, Japan. ADAR2 and DAT were cloned into EYFP vector (ClonTech). Human embryonic kidney 293 (HEK293) and MSR-29 cells (HEK-MSR-293, Invitrogen) were grown in RPMI1640 (61870, GIBCO) and Dulbecco's modified Eagles medium (DMEM, GIBCO), in both cases supplied with 10% fetal calf serum (FCS), and 1% pen/strep. In addition, HEK-MSR-293 cells were supplemented with 60 mg/ml geneticin and minimum essential medium (MEM). For transfection, cells were seeded on coverslips (#1.5, Menzel Gläser) which, for HEK 293, were coated with poly-L-lysine (P8920, Sigma Aldrich). Transient transfection with 1 or 2 μg of vector was performed 24 or 48 h prior to live-cell imaging or fixation using Fugene 6 (11 814 443 001, Roche), lipofectamine reagent (18324-012, Invitrogen) supplemented with Plus Reagent (10964-021, Invitrogen), or standard calcium-phosphate transfection (made stock in house). Cells were washed in phosphate-buffered saline (PBS) before fixation with 4 or 8% paraformaldehyde (#15710, Electron Microscopy Sciences) in PBS (10010, GIBCO), or with Lillie's fixative (VWR), for 15 to 30 min at room temperature. Fixed cells were mounted onto slides using Vecta Shield Hard Set mounting medium (H-1400, Vector Laboratories). Samples were not sealed with nail polish unless otherwise stated. Samples were left to dry (solidify) for a couple of hours at room temperature and were subsequently stored at 4 °C in the fridge unless otherwise stated. Before fluorescence imaging of live cells, the medium was replaced with DMEM without phenol red (GIBCO).

2.2 Fluorescence Microscopy

The following fixed samples, in addition to 10 EYFP-SERT live samples, were evaluated right after preparation (2 to 4 days after mounting): 7 EYFP-SERT, 2 EYFP-DAT, 8 EYFP-only, 5 Venus-only, and 30 ADAR2-EYFP samples, 10 of which were sealed with nail polish. For each of these samples, 514-nm fluorescence recovery after photobleaching (FRAP) or continuous bleaching time series (explained later in this section) from at least 5 different cells distributed over the sample were measured on the same day. A few of these samples were also evaluated at later times in addition to a few other fixed samples, which were not evaluated right after preparation (see Sec. 3).

Cells were examined on a Zeiss confocal laser scanning microscope (LSM) 510 META microscope using a 40× NA 1.2 C-Apochromat objective. For all measurements, the META detector was applied, either in bandpass or in spectral mode. Image parameters were adjusted on medium-level ECFP and EYFP-expressing cells. For bandpass imaging, laser powers were set to 20 μW with 458-nm and 3 μW with 514-nm excitation, as measured at the sample using a Thorlabs power meter (PM121; PM100 console with S121B Si sensor). On our microscope, this corresponded to acousto-optic filter (AOF) settings of 5% and 0.35%, at an Ar tube current setting of 50% (6.0 A). The laser power was measured, using the Spot Scan and Time Series features of the microscope, with a Zeiss 10× NA 0.30 EC Plan-Neofluar objective. The measurements were corrected with regard to transmission differences between the 10× and 40× objective, amounting to around 10%. Spectral fluorescence emission scans were acquired with 458-nm excitation only, using 28 or 55 μW for prebleach and 55 or 110 μW for postbleach scans. Bandpass and spectral imaging were performed with HFT 458/514 and NT 80/20 (20% reflectance, 80% transmittance), main dichroic filters, respectively, except for Fig. 4, where an HFT 405/514/594 filter was used for 405 nm bleaching. The data presented in Fig. 4 were acquired at a different Zeiss LSM 510 META microscope with an additional 405-nm laser that was not present on our own system. The microscopes are otherwise identical (purchased at the same time) and settings, including the type of objective, were kept the same on the two systems.

Pre-and postbleach images 512×512 pixels in size (37.5×37.5 μm) were acquired with pixel dwell time 6.4 μs (scan speed 6), 70 nm/pixel (scan zoom 6), and line average 1 or 2. These images were acquired with a four-channel configuration set up for sensitized acceptor emission FRET analysis: CFP emission with CFP excitation, YFP emission with CFP excitation, YFP emission with YFP excitation, and CFP emission with YFP excitation (back-bleedthrough control). Only the first and third channels were used for bleach and FRAP time series, from now on referred to as CFP and YFP channels. Bandpass measurements were performed with the META detector set to 469 to 501 nm and 533 to 576 nm. Spectral scans were acquired in the 453 to 699 nm range with 10.6-nm steps and 110 μW at 458 nm. The detector gain was set to 600 for CFP and 550 for YFP channel detection unless otherwise stated. Amplifier offsets and amplifier gains were set to 0.1 and 1, respectively. Pinholes were set to 1 Airy unit, corresponding to an optical slice thickness of 1.0 μm.
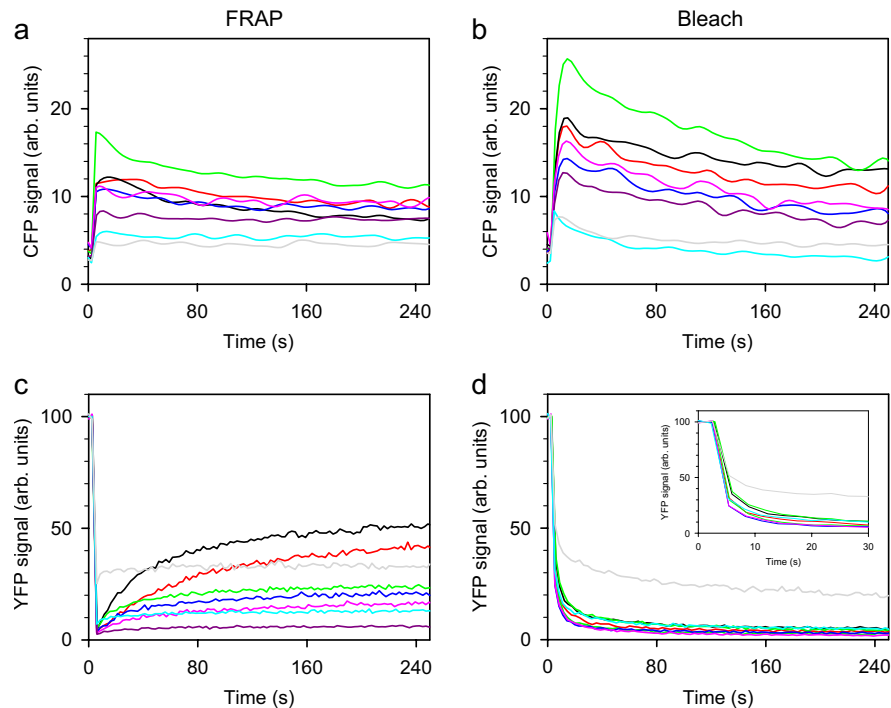
Fig. 1 Normalized 514-nm FRAP and bleach (175 μW) curves acquired in two different ROIs (0.5×0.5 μm^2) of the same cell for eight different cells within the same EYFP-only sample (one month old). (a) CFP-like signals acquired along with the EYFP signals shown in (c). (b) CFP-like signals acquired along with the EYFP signals shown in (d). Different colors represent different mobilities as evident from (c). (Color online only.)

In the following and elsewhere, "bleach curve" refers to a time series with alternating 514-nm YFP photobleaching and CFP/YFP channel detection, while FRAP refers to a time series with one intense 514-nm bleach event and subsequent CFP and YFP channel detection. For FRAP, a 7×7 pixel (0.5×0.5 μm) region of interest (ROI) was selected, while for bleaching, 7×7, 28×28, or 56×56 pixel ROIs were used. Average CFP and YFP channel signals within the ROI were collected using Time Series, Edit Bleach mode with Use ROI enabled within the Scan Control menu. In all cases, two prebleach data points were acquired, and the time series was terminated after 30 or 250 s. The 250-s scans were always checked for focal and lateral drifts, which were allowed to be 0.5 μm and 2 pixels (0.14 μm) at most, respectively, during this time interval. For bleach curves, a 514-nm bleach power of 175 μW was most frequently used, corresponding to an AOF transmission of 17.5% with 50% Ar tube current. Powers were checked several times over several weeks of measurement sessions and were allowed to vary at most 10%. For FRAP, the Argon tube current was increased to 100% (8.0 A) and the ROI bleached once, using 16 iterations, pixel dwell time 6.4 μs, and 100% 514-nm AOF line transmission, corresponding to 2.5 mW at the sample. Note that this value is roughly 16 times 175 μW. For bleach curves, a pixel dwell time of 102.4 μs (scan speed 2) and 1 iteration was applied unless otherwise stated. It was discovered during the experiments that an "intrinsic" time delay of ~2 s was added for each data point due to an unintentional mechanical filter shift in a Confocor module attached to our system. This resulted in a ~3 s time delay per data point despite no user-defined time delay being added in the time series. The filter shift happened

even though the Confocor module was not at all activated or in any other way related to the experiment. All images were acquired as 8-bit (256 intensity levels).

For acquisition of EYFP bleach curves at variable wavelengths (Fig. 5), employing 458-, 514-, 543-, and 633-nm bleaching, an HFT 458/543/633 main dichroic beamsplitter was used in addition to the HFT 458/514. To facilitate a quantitative comparison of the signals acquired with the two different dichroics, detector gains were readjusted using enhanced CFP (ECFP)–only and EYFP-only samples in order to compensate for the difference in detection efficiency in the CFP and YFP channels, caused by differences in the dichroic filter transmissions. This resulted in optimum detector gains of 645 for the CFP and 625 for the YFP channel. Imaging in the YFP channel in this case had to be performed with 458-nm excitation due to the absence of a main dichroic beamsplitter with 458-, and 514-nm excitation together with 543 or 633 nm. Also, the absence of a main dichroic beamsplitter with 458-nm as well as 488-nm reflection prevented the investigation of photoconversion at the 488-nm wavelength. For all the wavelengths investigated, the bleach laser power was adjusted to 175 μW at the sample. For imaging, 20-μW 458-nm laser power was used for the YFP as well as the CFP channel.

For EYFP bleaching under wide-field conditions, the light from a 100-W HBO Mercury lamp was deflected onto the sample by means of a z514/10 excitation filter and a 535DCXR dichroic filter (Chroma Technology), admitting light in the 509 to 519-nm range. The light beam was apertured down to a diameter of ~57 μm on the sample, corresponding to a power of 60 μW, i.e., an intensity of
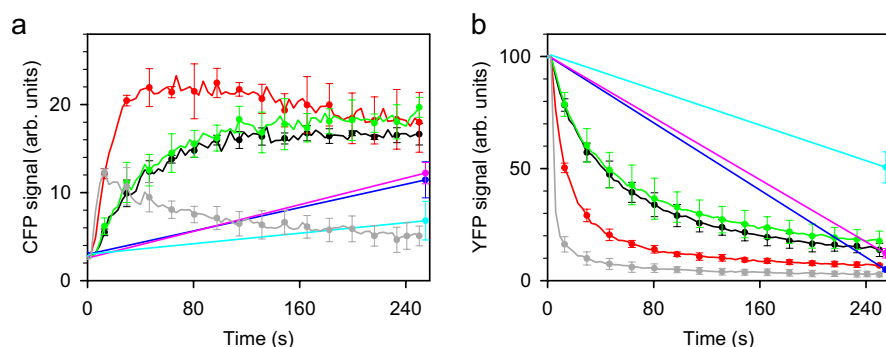
Fig. 2 Normalized 514-nm bleach curves ($0.5 \times 0.5 \ \mu m^2$ ROIs) acquired three days after mounting for a EYFP-DAT sample, showing the effect of bleach power, bleach scan speed, and number of bleach iterations. (a) CFP-like signals corresponding to the EYFP signals shown in (b). Dark gray: 175-μW bleach power, pixel dwell time 102.4 μs, and 1 bleach scan iteration. Black: 11-μW bleach power, pixel dwell time 102.4 μs, and 1 iteration. Red: 175-μW bleach power, pixel dwell time 6.4 μs, and 1 iteration. Green: 11-μW bleach power, pixel dwell time 6.4 μs, and 16 iterations. Blue: 11 μW, 102.4 μs, and 580 iterations. Pink: 3 μW, 102.4 μs, and 580 iterations. Cyan: 0.5 μW, 102.4 μs, and 580 iterations. Signals have been normalized with regard to EYFP prebleach signal levels and time axes of the dark gray, black, and red curves have been slightly "stretched" in order to account for the time delay introduced by the difference in number of bleach scan iterations. 0.5 μW is the absolutely lowest 514-nm laser power that can be applied to the sample without technical modifications to our microscope system (such as misalignment of the optical fiber or insertion of a gray filter). (Color online only.)

23 kW/cm^2. This is much less than the intensity used for bleaching in the confocal scanning mode with the 514-nm laser line, amounting to at least 223 MW/cm^2 at 175 μW, assuming (conservatively) a 1-μm-diam laser beam spot on the sample. The HBO lamp power at the sample was found to be very sensitive to the positioning of the lamp focus knob and was always checked prior to a measurement session. For wide-field bleaching, a pre-and postconfocal image was acquired under similar conditions, as described earlier. HBO illumination was initiated and terminated by switching forth and back from VIS mode in the LSM software. HBO illumination times of 5, 15, or 30 min were applied. The extent of focal drift taking place during illumination was estimated from additional pre-and postconfocal overview images covering an area of $225 \times 225 \ \mu$m sample, from which the diameter of the HBO illumination spot could also be determined.

2.3 Data Analysis

FRAP and bleach curves were background-subtracted, and signals in the CFP and YFP channels were normalized with regard to an average of the two YFP prebleach data points. For background subtraction, the minimum values in the CFP and YFP channels of the preimage, as obtained by means of the Histogram feature in the LSM software, were used. This was found to be more reliable compared to an average over an extracellular region, which sometimes resulted in negative values. Bleedthrough contributions of CFP-like signal into the YFP channel and vice versa were not corrected, as these were considered insignificant for the META detector. For each sample and illumination condition, 3 to 5 curves were selected on the basis of the drift criteria (see the preceding) and represented as one single average curve with error bars reflecting plus one and minus one standard deviation. In Fig. 1, as well as for the spectral scans, only single nonaveraged curves are shown, and thus no error bars have been included. In Fig. 1, in order to visualize the differences between the curves, the CFP-like signals have been smoothed using a bisquare algorithm with sampling proportion 0.25 and polynomial degree 5 (SigmaPlot version 10.0, Systat Software). Spectral scans are shown as spline curves.

3 Results

In order to examine whether our samples were prone to EYFP photoconversion and in order to quantify the magnitude of the effect, 10 living samples of EYFP-SERT were examined in addition to a large number of fixed samples transfected with EYFP-SERT, EYFP-DAT, EYFP-only, Venus-only, and ADAR2-EYFP. The samples were evaluated on a Zeiss LSM 510 confocal microscope, and the extent of photoconversion was quantified as the rise in average signal in the CFP channel within a small region of interest (ROI) bleached with 514-nm confocal laser light illumination unless otherwise stated. EYFP photoconversion was observed mainly in the fixed, nonsealed EYFP-transfected samples, with the CFP-like signal rising up to 15 intensity units on a normalized intensity scale (100 units corresponding to the prebleach EYFP level) for samples examined within 5 days of mounting, using 175-μW bleach power and bleach scan speed 2 (see Sec. 2). Photoconversion was observed only to a minor extent in living cell samples, being present in 2 (out of 10) samples, which were transfected on the same day. In one sample, 6 cells were evaluated, and the CFP-like peak was observed in all of them to a level of around 10 intensity units (175-μW bleach power). In the other sample, 3 out of 10 cells examined showed a very mild conversion, with the CFP-like signal not exceeding $\sim$2 intensity units. For fixed, nonsealed Venus-only samples, 4 out of 5 samples did not show any signs of photoconversion, and in the remaining sample, in 4 out of 9 cells, a mild conversion was observed, with the CFP-like peak increasing at most 4 normalized intensity units (175-μW bleach power).

We did not observe any dependence on the transfection time (24 versus 48 h), amount of vector (1 versus 2 μg), or cell line applied; photoconversion also was observed in
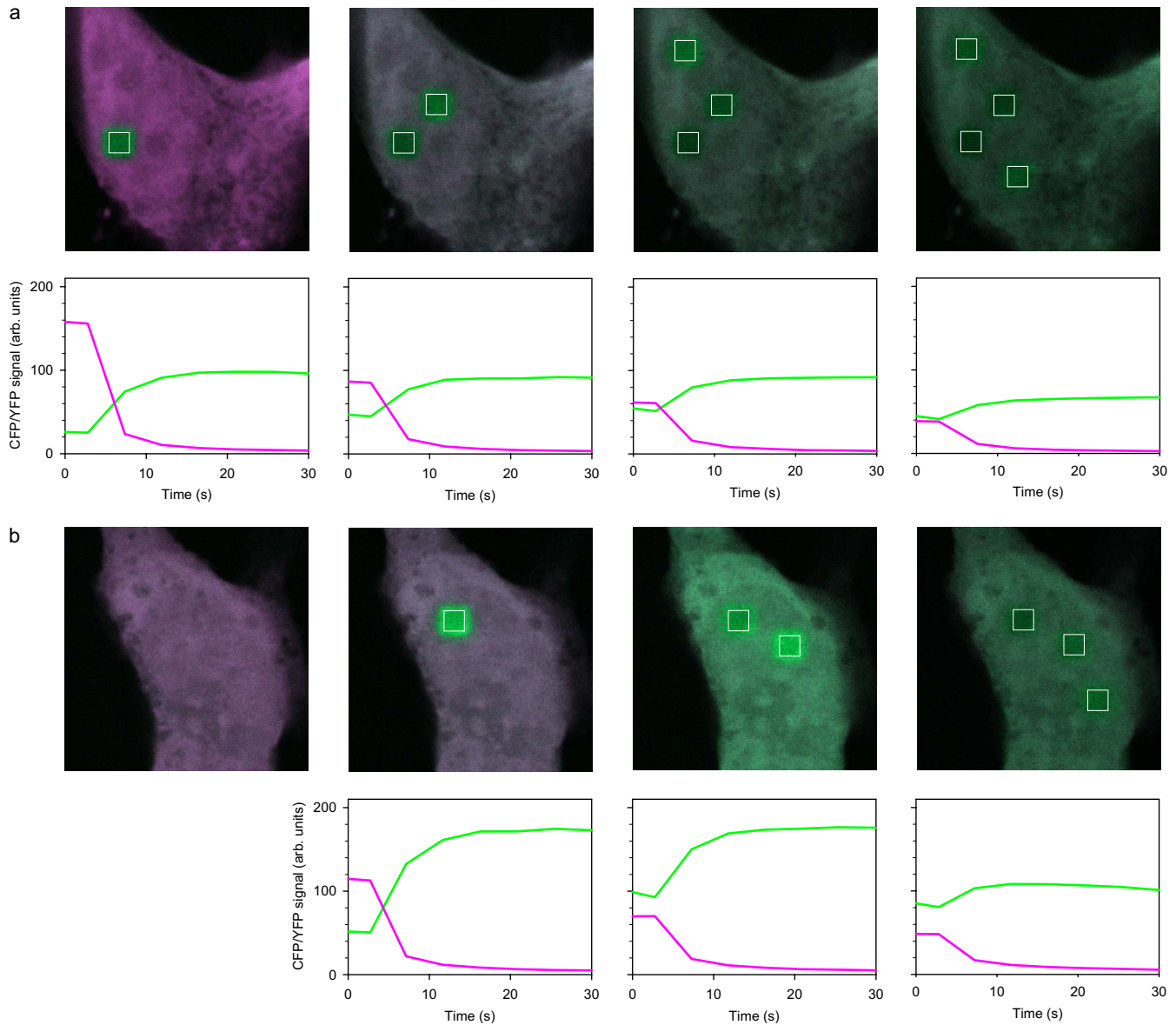
Fig. 3 Image series of EYFP-only cells (4-month-old sample) showing the effect of subsequent 514-nm, 175-μW bleaching of different ROIs (2 $\times 2$ μm²) within a single cell, interspersed with 458-nm exposures at 110 μW (laser power applied for spectral postbleach scans). Prebleach CFP-like (green) and EYFP (pink) signals are seen to gradually increase and decrease, respectively, from left to right, indicating that photoconversion is inducible also with 458-nm illumination. Note that the level of CFP-like signal reached during 514-nm bleaching is almost unaffected by the decrease in prebleach EYFP signal in the first three images. (The variation in EYFP expression level is limited to ±5% among the ROIs.) (Color online only.)

EYFP-SERT transfected Cos-1 and SHSY5Y cells. What we did find, however, was a propensity for sealed samples with overall more diffusion present as examined by FRAP to exhibit overall smaller conversion efficiencies. Figure 1 shows selected FRAP and continuous bleaching time series (hereafter referred to as "bleach curves;" see Sec. 2) for different cells within one particular EYFP-only sample. As can be seen, there is a large variability in the speed of diffusion (reflected in the slopes of the postbleach curves) and fraction of immobile molecules (reflected in the "amplitude" of recovery). In some samples, almost full recovery was observed for many cells within a few seconds, and it was not possible to find cells with a diffusion level limited to that of the purple or

cyan curves in Fig. 1(c) (data not shown). In those cases, a CFP-like peak was detected only transiently in the FRAP measurement, with the amplitude being anticorrelated with the dip in the EYFP signal with some amount of long-time CFP-like signal remaining, correlated with the fraction of immobile EYFP. These observations demonstrate that EYFP photoconversion does not correlate with the fixation state as such at the cellular level. Largest mobility was found for newly mounted samples sealed with nail polish, in particular for EYFP-only and Venus-only, while for ~3-month-old samples, hardly any diffusion was left. These samples also showed signs of drying from a visual inspection of the mount-
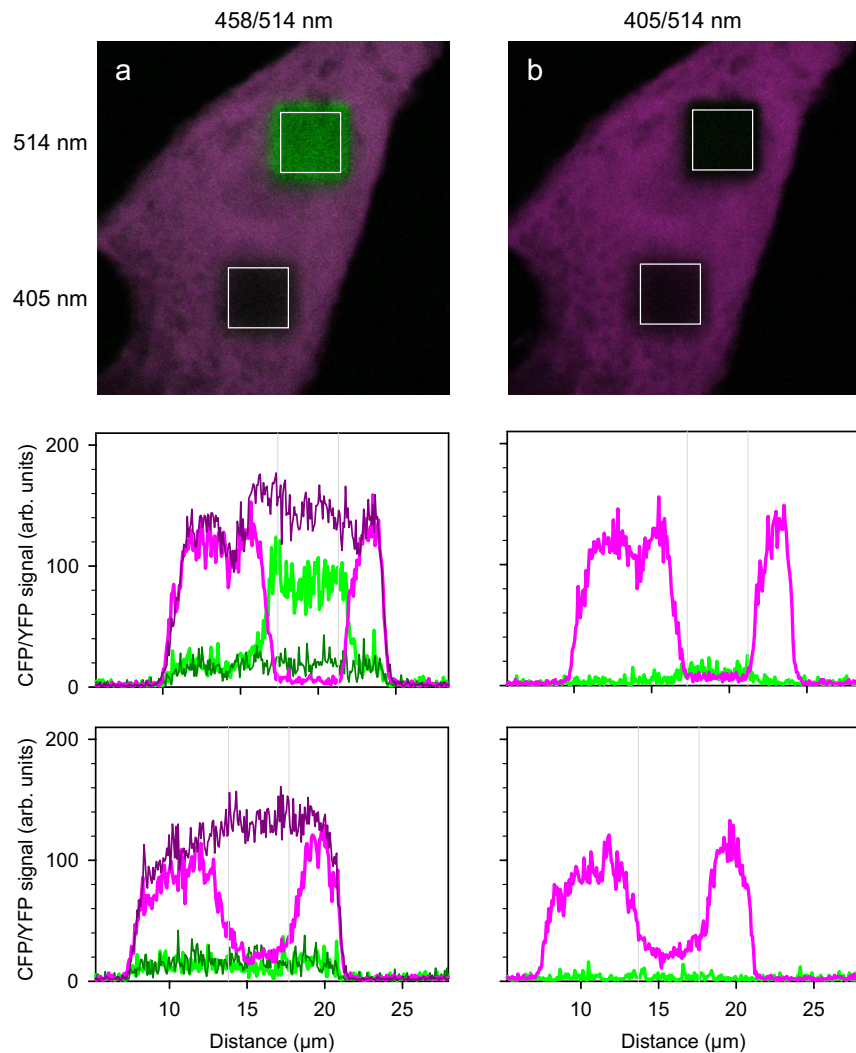
Fig. 4 Images of a fixed EYFP-only cell (3-month-old sample) acquired with (a) 458/514-nm and (b) 405/514-nm excitation following 30 s of 175-μW, 514-nm (upper ROI) and ~165-μW, 405-nm (lower ROI) bleaching of a 4×4 μm^2 (56×56 pixels) area. Corresponding cross sections are shown below each image with purple and pink indicating EYFP signals before and after 514-nm bleaching. Dark green and green indicate CFP-like signal before and after (a) 458-nm and (b) 405-nm bleaching. (Color online only.)

ing medium. In the living EYFP-SERT samples, relatively little EYFP-SERT mobility was observed. As can be seen in Figs. 1(a) and 1(c), there is no clear correlation between the amplitude of the CFP-like peak and the fraction of immobile EYFP. It can also be seen that the CFP-like peak is lower for FRAP compared to bleach curves, which can be attributed to bleaching of the CFP-like species during the FRAP bleach shot due to the higher laser power and number of bleach scan iterations despite a lower pixel dwell time.

Next, we examined whether it was possible to find illumination conditions under which YFP photoconversion could be suppressed, and we tried to vary the laser power, pixel dwell time, and number of bleach iterations. Figure 2(a) shows CFP-like signals corresponding to the EYFP signals given in Fig. 2(b) under different bleaching conditions for a one-month-old EYFP-DAT sample. The black, red, and green curves in Fig. 2 have been acquired with the same laser fluence, i.e., the laser power, pixel dwell time, and iteration number have been varied such that the same total amount of en-

ergy has been delivered to the sample within the 250 s of total acqusition time. The red curves have been acquired with 175 μW of bleach laser power (1 iteration, pixel dwell time 6.4 μs)—16 times higher than the 11 μW applied for the black and green curves, which on the other hand have been bleached with 16 times higher pixel dwell time and 16 bleach scan iterations, respectively. As seen in Fig. 2, the CFP-like species develops slower at the lower laser powers but with EYFP also bleaching correspondingly slower. The correlation of the rate of CFP-like species formation with the rate of EYFP decay is direct evidence that the CFP-like species is indeed originating from EYFP. For the same amount of fluence being deposited (black, red, and green curves), photoconversion develops faster at the highest laser power (red curve), which is indicative of a thermal effect, as the sample is transiently heated to higher temperatures at the higher laser power applied. The cyan, pink, and blue curves of Fig. 2 were acquired with ~0.5 μW, 3 μW, and 11 μW of laser power,
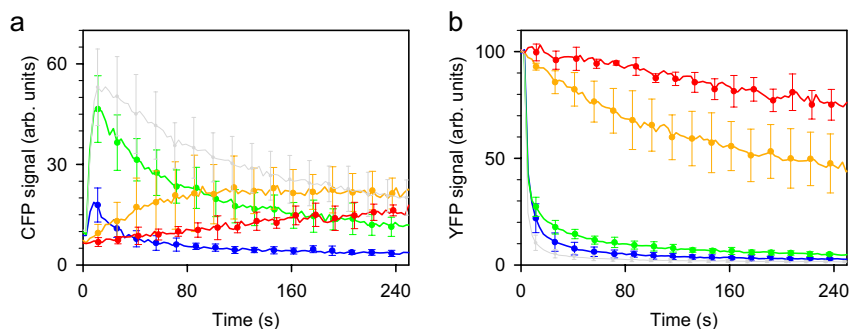
Fig. 5 Influence of laser bleach wavelength on EYFP photoconversion and bleaching decay rate for a EYFP-DAT sample measured on the same day one month after mounting (0.5×0.5 μm^2 ROIs). (a) CFP-like signals corresponding to the EYFP signals shown in (b). Signals have been normalized wrt. EYFP prebleach signal levels. Blue: 458 nm; green: 514 nm; yellow: 543 nm; red: 633 nm; and gray: 514 nm, acquired one day in advance under slightly different EYFP imaging conditions (using 514-nm excitation; see Sec. 2). Since identical settings were used for recording of the CFP-like signal, the green and gray curves in (a) in principle should be identical; the discrepancy is due to the environmental effects acting across the sample and as a function of storage time. (Color online only.)

respectively, using 580 bleach scan iterations and a pixel dwell time 102.4 μs. This number of iterations was chosen in order to result in 250 s of continuous scanning within the ROI. 0.5 μW is the absolutely lowest 514-nm laser power that can be applied to the sample without technical modifications to our microscope system (such as misalignment of the optical fiber or insertion of a gray filter). The CFP-like species is seen to develop much slower in these cases, again correlated with a slower EYFP decay.

Highest conversion efficiencies were detected in a few 3 to 4-month-old nonsealed samples transfected on the same day and stored at 4 °C. Unfortunately, none of these samples were among the ones evaluated right after mounting. Those samples exhibited a large variation in conversion efficiency across the sample, and most cells were already to some extent preconverted prior to confocal examination. Examples of 514-nm bleach time series interspersed with 458-nm excited fluorescence emission spectral scans for one of these samples is shown in Fig. 3. The second image of the series, shown in Fig. 3(b) depicts the highest CFP-like signal that was observed by us (around 150 normalized intensity units), corresponding to the highest apparent conversion efficiency detected. As seen from the relatively high prebleach level of CFP-like signal, some preconversion had already taken place for this cell, making a precise estimate of the conversion efficiency difficult. For the same reason, bleach curves, showing signs of preconversion, have not been normalized. However, as the images have been acquired with the laser power and detector settings optimized for detection of a medium-level expression of ECFP (adjusted using an ECFP-transfected sample), the brightness of the CFP-like species is seen to be comparable to that of ECFP. Photoconversion was found to be inducible to a minor extent also with 458-nm illumination, as is evident from the gradual increase and decrease of the prebleach signals in the CFP and YFP channels, respectively, when proceeding from left to right through the image series of Fig. 3. Perhaps more interesting, the level of CFP-like signal reached during 514-nm bleaching was not much affected by the decrease in prebleach EYFP signal, indicating that the subpopulation of EYFP proteins most easily bleached by 458-nm illumination are the most efficient 514-nm converters.

Bleach time series were acquired also with 405-nm light at ~165 μW, but in this case, no conversion was observed, and also no absorption of the CFP-like species could be detected at this wavelength (Fig. 4). As is evident from Fig. 4(a) (image and cross sections), regions of EYFP bleaching and photoconversion are extending at least 0.5 μm beyond the boundaries of the predefined ROI. The extent to which a bleached area was growing beyond the predefined ROI boundaries was seen to increase with increasing length of the bleach time series (data not shown). These observations are further evidence for a thermal effect. No regeneration of EYFP from the CFP-like species upon illumination with 175 μW of 405-nm laser power was observed (two cells in each of two different samples), but the CFP-like species was efficiently bleached on a 30-s time scale at this wavelength (Fig. 4). Examined at other bleach wavelengths, EYFP bleaching and accompanying photoconversion were observed to develop also at 543 and 633 nm, albeit at a lower rate compared to 514 nm, for similar laser powers (cf. Fig. 5). Photoconversion is seen to happen much faster at 458 and 514 nm, but the CFP-like peak does not reach as high a level with 458 nm, which could be due to faster bleaching of the CFP-like species at 458 nm (given its higher absorption at this wavelength). Alternative EYFP decay channels also might play a role, as supported by the faster EYFP decay with 458-nm as compared to 514-nm bleaching. The fact that photoconversion happens to a significant extent also with 543- and 633-nm illumination is again evidence for a thermal effect.

In order to examine the influence of storage time (4 °C) on photoconversion, 4 EYFP-SERT and 2 EYFP-DAT nonsealed samples were evaluated every one or two months after preparation, but it was not possible to detect any general trend in the photoconversion behavior (Fig. 6). The photoconversion efficiency was highly variable as a function of time, with some samples exhibiting a large increase, others a decrease at different times. In order to examine further the effects of temperature and diffusion, a batch of ADAR2-EYFP samples, consisting of 10 samples transfected on the same day, with 5 being sealed (using nail polish) and 5 left unsealed, were compared. All samples were evaluated by FRAP 2 days after mounting, at which time there already was a higher conver-
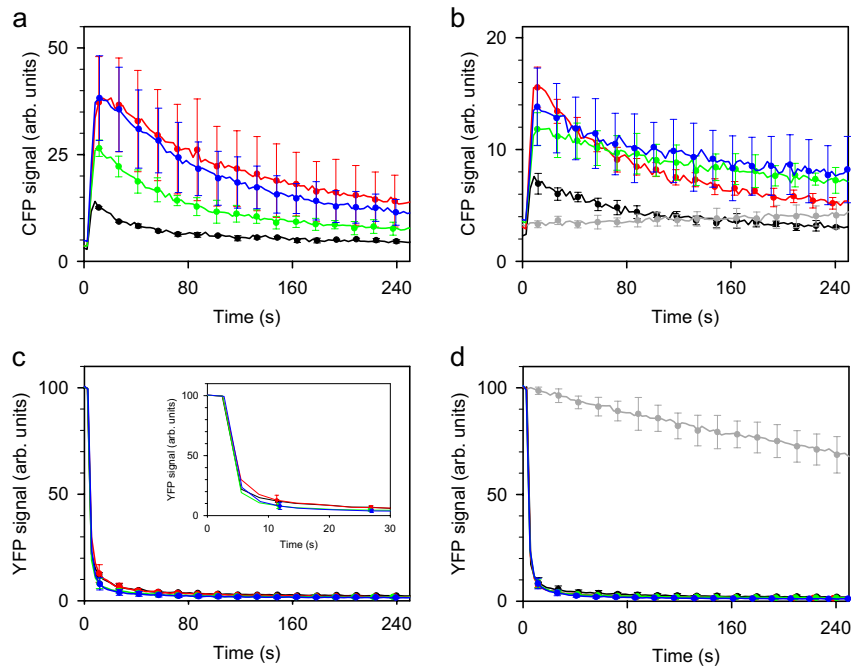
Fig. 6 Examples of normalized 514-nm bleach curves (0.5×0.5 μm^2 ROIs) for EYFP-SERT measured as a function of sample storage time (4 °C) for two different samples transfected at different dates. (a) and (b) CFP-like signals corresponding to the EYFP signals shown in (c) and (d). Measurements were performed three days after mounting (black), one month later (red), two months later (green), and three months later (blue). The dark gray curves in (b) and (d) represent a measurement three days after mounting with zero bleach power. (Color online only.)
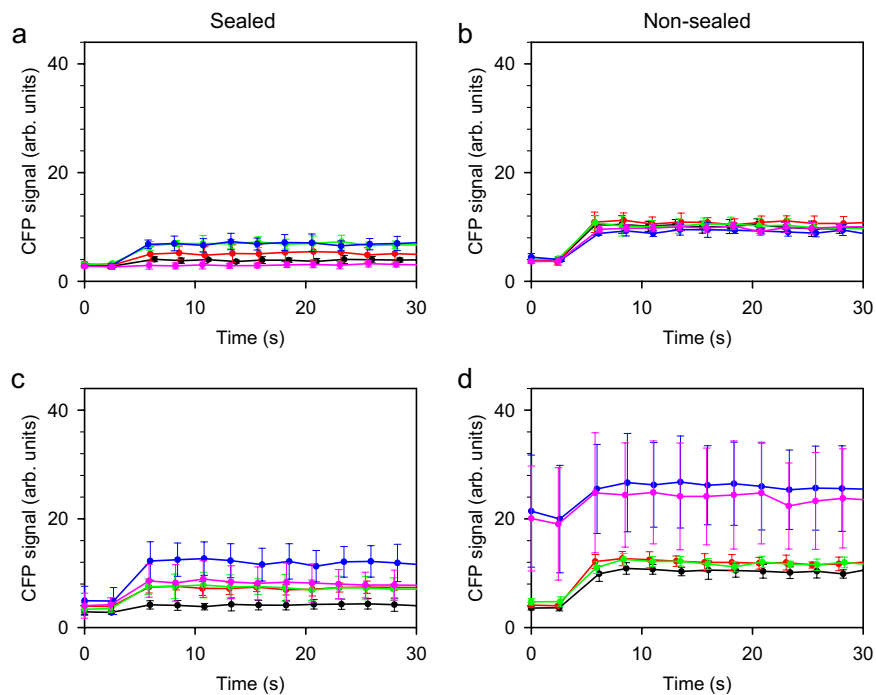
Fig. 7 Influence of sealing (nail polish) and storage conditions on EYFP photoconversion induced by 514-nm FRAP (0.5×0.5 μm^2 ROIs) for 10 fixed ADAR2-EYFP cells (5 sealed, 5 nonsealed; transfected and mounted simultaneously). Each curve represents one sample: (a) sealed and (b) nonsealed samples measured two days after mounting; (c) and (d) samples from (a) and (b) after 36 h at 4 °C (black), at room temperature (red, green), and at 60 °C (blue, pink). Signals have been normalized wrt. EYFP prebleach signal levels. (Color online only.)
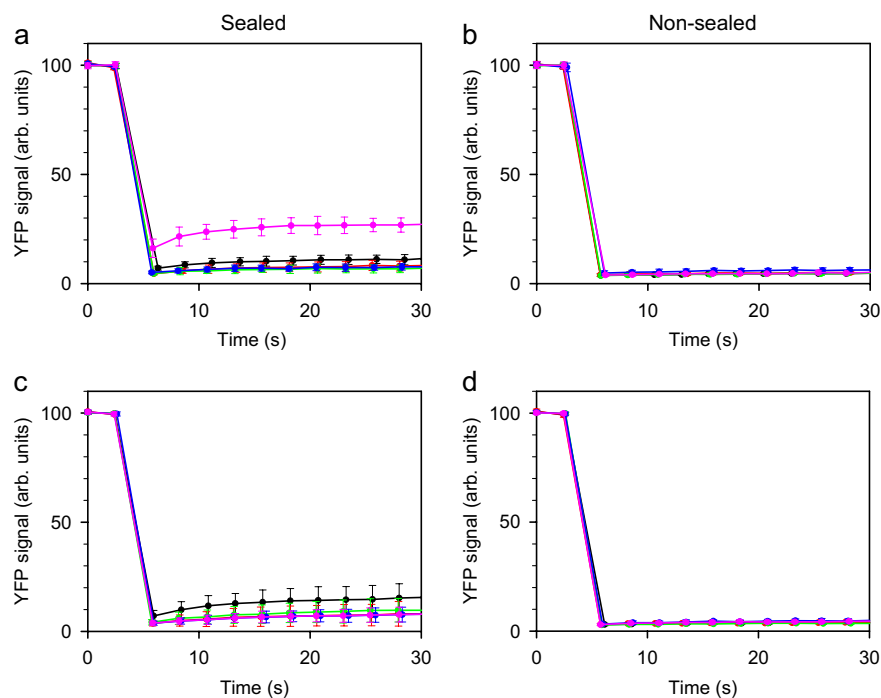
Fig. 8 Normalized EYFP signals from the FRAP time series giving rise to the CFP-like signals shown in Fig. 7 (0.5×0.5 μm² ROIs). Sealed samples are seen to be slightly diffusive, whereas no diffusion is present in the nonsealed samples.

sion efficiency among the nonsealed compared to the sealed samples (Figs. 7 and 8). This trend was amplified after 36 h of storage under different temperatures: at 4 °C in the dark (2 samples), at room temperature in the dark (4 samples) and at 60 °C in an oven in the dark (4 samples). The nonsealed samples clearly had higher conversion efficiencies as compared to the sealed samples, and among the nonsealed samples, there was a significant increase in conversion efficiency for the samples stored at 60 °C compared to the samples stored at lower temperatures (Figs. 7 and 8). Those samples also appeared significantly drier from a visual inspection. Figure 9 shows two examples of cells from one of the nonsealed ADAR2-EYFP samples stored for 36 h at 60 °C; one cell has photoconverted partially (a) while the other has photoconverted completely (b) during this time period at this temperature. The CFP-like species is seen to be relatively photostable, showing only a minor degree of bleaching after 250 s of imaging using laser power and detector settings adjusted for imaging of medium-level CFP-expressing cells. From corresponding spectral scans, the fluorescence spectrum of the CFP-like species was found to be dominated by a 500-nm peak with a 525-nm shoulder, which is reminiscent of the EYFP main fluorescence peak (Fig. 9; see also Fig. 10). Sometimes the 525-nm peak was found to dominate the 500-nm peak, giving rise to spectra like the one shown in the right part of Fig. 10, which is a remeasurement (at a later time) of the spectrum shown to the left. However, this can be explained by residual EYFP diffusion into the ROI during or after bleaching (but before the spectral scan), as also illustrated in the cross section of the figure. Those residual EYFP molecules will give a relatively large contribution to the spectrum at 500 nm.

Last, we investigated the extent of EYFP photoconversion taking place under wide-field as compared to confocal illumination conditions. Figure 11 shows an EYFP-only cell subjected to 30 min of wide-field bleaching by means of an HBO Mercury lamp (60 μW in the 509 to 519-nm spectral range; note that power is very sensitive to arc lamp focal position), following 30 s of confocal bleach time series acquisition of a 2×2 μm² ROI with 175 μW at 514 nm. As seen from the images and corresponding cross sections, a much smaller fraction of EYFP is converted to the CFP-like species with wide-field as compared to confocal bleaching.

4 Discussion

Our results provide evidence that EYFP photoconversion can be explained by a thermal effect that seems to be enhanced at 514 nm and thus may be associated with a hot vibrational level of the ground state or an electronically excited state of EYFP. The strong negative correlation of the conversion efficiency with the amount of diffusion present in the sample is evidence that dehydration and/or oxygenation of the sample are major risk factors for the susceptibility of fixed EYFP samples toward photoconversion. The fact that photoconversion also appears in a minor fraction of the living cell samples points toward the maturation of EYFP at the cellular level as another factor, which may play a smaller role. On average, the mobility of molecules (EYFP, water, oxygen, etc.) in a fixed sample is lower than in a living sample, which means that heat deposited in the illumination spot and chemical reactants generated there are less efficiently carried away. This causes a higher temperature increase compared to a living sample with a more aqueous environment with a higher heat capacity. The
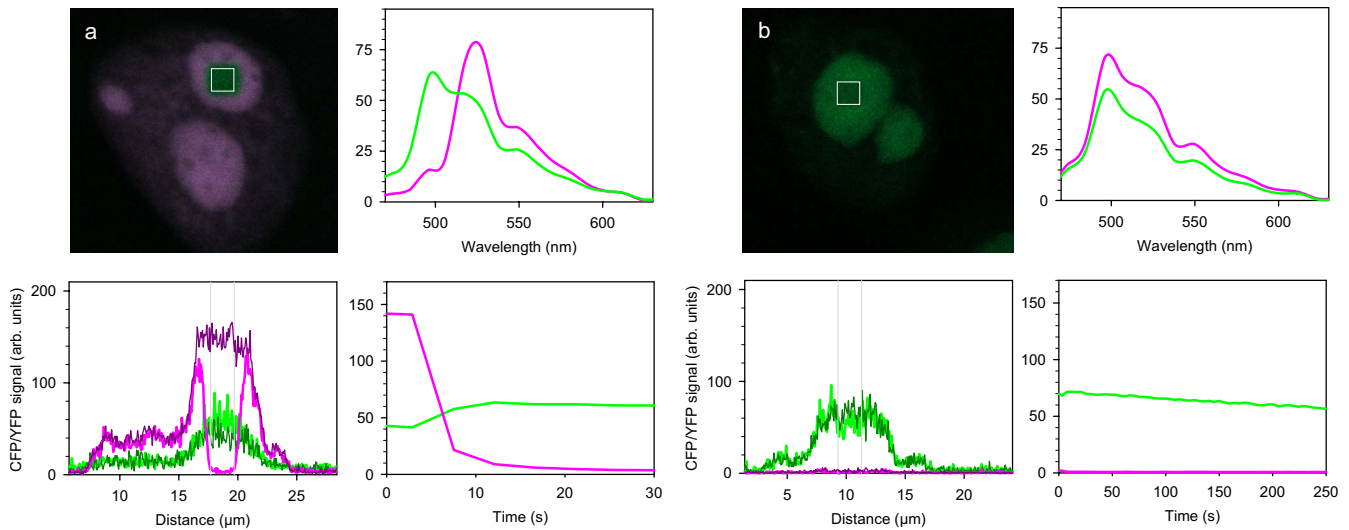
Fig. 9 Images of fixed ADAR-EYFP cells (a) partially and (b) fully converted to CFP-like species after 36 h of storage at 60 °C and subsequently subjected to 30 s of 514-nm bleaching ($2 \times 2 \ \mu m^2$ ROI). Each image is accompanied by three curves. Upper right: Fluorescence emission spectrum before (pink) and after (green) bleaching. Prebleach spectra were acquired with 28 μW (left) and 55 μW (right), while postbleach spectra were acquired with 110 μW at 458 nm. Lower left: EYFP signal before (purple), EYFP signal after (pink), CFP-like signal before (dark green), and CFP-like signal after (green) bleaching. Lower right: Associated EYFP (pink) and CFP-like (green) signals as a function of time. (Color online only.)
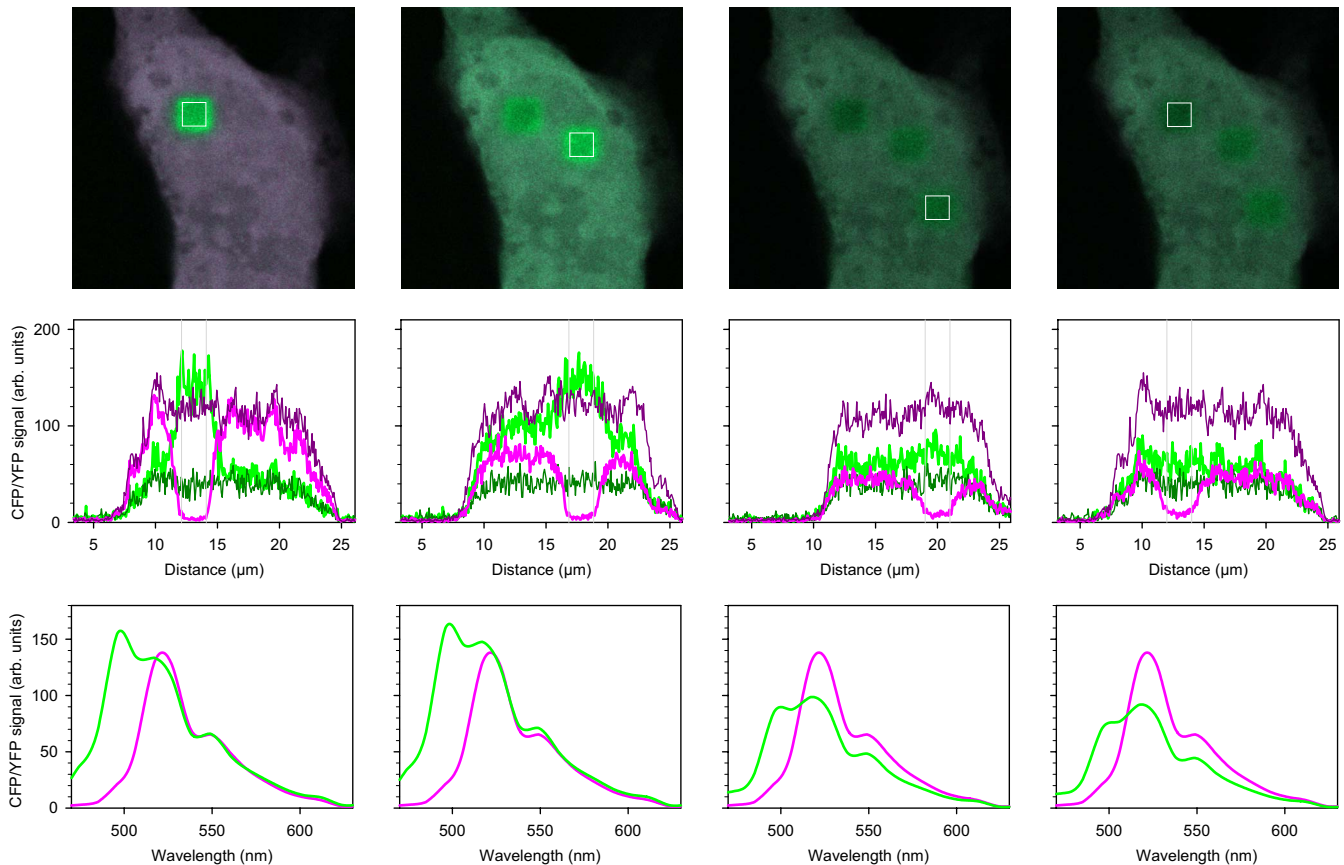
Fig. 10 Image series of a fixed EYFP-only cell [same as in Fig. 3(b)] with associated cross sections and spectral scans acquired during four 514-nm bleach time series interspersed with spectral fluorescence emission scans, showing the effect of residual EYFP diffusion on the apparent relative heights of the 500- and 525-nm peaks. For cross sections, purple and pink indicate EYFP signal before and after bleaching, with dark green and green indicating the corresponding levels of CFP-like signal. For spectral scans, pink and green represent pre- and postbleach acquisitions, respectively. (Color online only.)
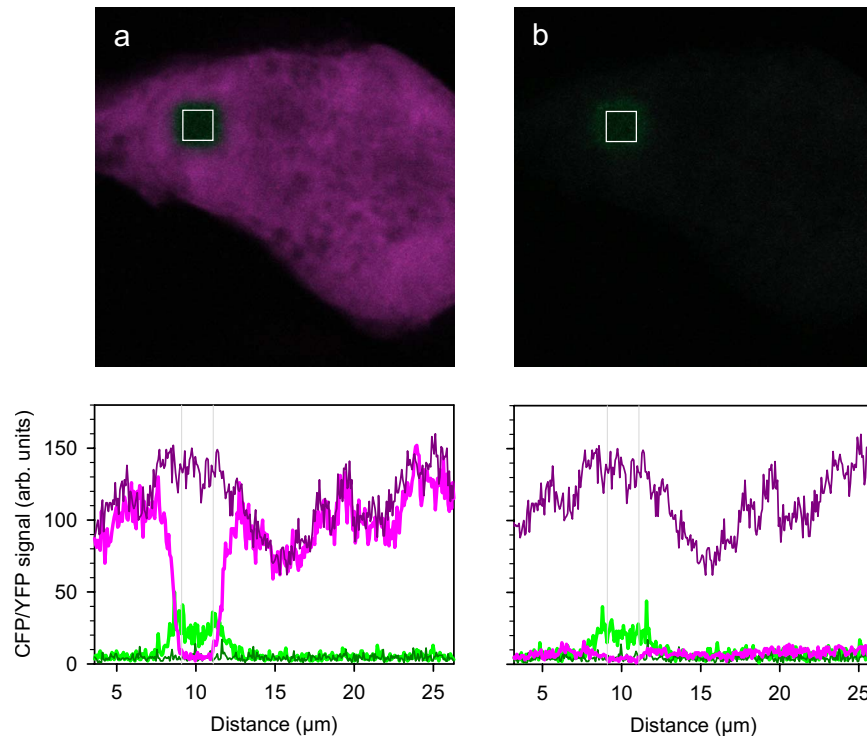
Fig. 11 Images of an EYFP-only cell (2-week-old sample) exposed to (a) 30 s of 514-nm bleaching at 175 μW (2×2 μm^2 ROI) and subsequently (b) 30 minutes of wide-field illumination with an HBO Mercury lamp in the 509 to 519-nm range, and (c) and (d) corresponding cross sections through the bleached area. Pink: EYFP signal; green: CFP-like signal. (Color online only.)

actual on-time of bleach laser light during the confocal photobleaching cannot be precisely estimated, but the bleach time periods are likely to be much shorter than the off-time periods. It may be that the enhancement of photoconversion at 514-nm bleach wavelength is a factor that is acting indirectly, e.g., being amplified by temperature and/or laser power and thus being suppressed under wide-field bleaching conditions. As the bleaching intensity (or pixel dwell time) increases, the time spent in the lowest-lying triplet state also increases, whereby the likelihood of singlet oxygen generation increases in addition to the probability for further excitation to higher-lying triplet states.[5,6] Maybe the generation of reactive-oxygen species is affecting EYFP in a manner that makes it prone toward entering the photoconvertible state. Although the fluorescent chromophore is highly shielded by its own protein environment, fluorescent proteins have been shown to be susceptible anyway to oxidative damage,[7] which alters the fluorescent protein structure.[8]

Many fluorescent proteins, including EYFP, have been found to exist in an equilibrium between a protonated, neutral (A) form and a nonprotonated, anionic (B) fluorescent form with absorption maxima at ~400 and ~500 nm, respectively.[9,10] Most highly populated under neutral pH is the B form, which is also mainly responsible for the fluorescence of these species. Regeneration of bleached EYFP by means of 330 to 390-nm, but only insignificantly by 395-nm illumination has previously been reported.[9,11] Likewise, we did not observe any absorption of the CFP-like species at 405 nm, nor any regeneration of EYFP at this wavelength (at 175 μW of 405-nm laser power), implying that the photoconversion does not involve transition to the neutral form. It also seems

unlikely that EYFP photoconversion should be linked to decarboxylation of the glutamate residue at position 222, as suggested by Valentin et al.,[2] as this has only been proposed in connection with A- to -B state conversion, not vice versa.[12]

Our observations and the preceding considerations at least partially explain the apparent controversy regarding the absence or presence of YFP photoconversion.[2–4] The fact that we only to a minor extent observe photoconversion in Venus-only samples prepared under exactly the same conditions as photoconvertable EYFP-only samples is in reasonable agreement with the observations by Valentin et al. Their level of Venus conversion also is less than that of EYFP, in particular when visualizing the CFP-like species with 458-nm excitation (Fig. S1 in Ref. 2). Interestingly, for EYFP as well as Venus, their CFP-like species seems to be absorbing at 405 nm and even appears brighter with 405-nm as compared to 458-nm excitation. This observation contradicts our studies, in which the CFP-like species is virtually non-absorbent at 405 nm (Fig. 4).

In summary, EYFP photoconversion to a CFP-like species is observed mainly in fixed, nonsealed cell samples for which the photoconversion efficiency exhibits a strong dependence on the hydration and/or oxygenation state of the sample. Photoconversion is thermal and, thus, less likely to develop under wide-field as opposed to confocal bleaching conditions. Given the large variations in conversion efficiencies observed among samples, within a given sample and as a function of storage time, photoconversion cannot be appropriately accounted for in the analysis of acceptor photobleaching FRET images. Thus, donor and acceptor controls should always be prepared in the same batch as the FRET samples and carefully checked

and discarded if photoconversion is present. We also recommend that samples are checked for EYFP diffusion, as there may be large variations in fixation efficiency from cell to cell within a sample as well as dependencies on mounting medium used, protein species coupled to EYFP, and age of the sample. It might be that the more hardening mounting media (e.g., Vectashield) facilitate less diffusion, i.e., better apparent fixation, but also higher photoconversion efficiency, which is something that needs further investigation. Last, based on the highly bright CFP-like signal observed in some of our samples, we point out the prospect for the development of blue-shifting photoconvertible fluorescent proteins based on green light illumination of mutated EYFP variants.

Acknowledgments

References

1. N. C. Shaner, G. H. Patterson, and M. W. Davidson, "Advances in fluorescent protein technology," *J. Cell. Sci.* **120**, 4247–4260 (2007).
2. G. Valentin, C. Verheggen, T. Piolot, H. Neel, M. Coppey-Moisan, and E. Bertrand, "Photoconversion of YFP into a CFP-like species during acceptor photobleaching FRET experiments," *Nat. Methods* **2**, 801–801 (2005).
3. M. T. Kirber, K. Chen, and J. F. Kearney Jr., "YFP photoconversion revisited: confirmation of the CFP-like species," *Nat. Methods* **4**, 767–768 (2007).
4. C. Thaler, S. S. Vogel, S. R. Ikeda, H. Chen, S. E. Verrier, and H.-D. Sölling, "Photobleaching of YFP does not produce a CFP-like species that affects FRET measurements," *Nat. Methods* **3**, 491–492 (2006).
5. R. T. Borlinghaus, "High speed scanning has the potential to increase fluorescence yield and to reduce photobleaching," *Microsc. Res. Tech.* **69**, 689–692 (2006).
6. M. J. Davies and R. J. W. Truscott, "Photo-oxidation of proteins and its role in cataractogenesis," *J. Photochem. Photobiol., B* **63**, 114–125 (2001).
7. L. Greenbaum, C. Rothmann, R. Lavie, and Z. Malik, "Green fluorescent protein photobleaching: a model for protein damage by endogenous and exogenous singlet oxygen," *Biol. Chem.* **381**, 1251–1258 (2000).
8. F. Bou-Abdallah and N. D. Chasteen, "Quenching of superoxide radicals by green fluorescent protein," *Biochim. Biophys. Acta* **1760**, 1690–1695 (2006).
9. T. B. McAnaney, W. Zeng, C. F. Doe, N. Bhanji, S. Wakelin, D. S. Pearson, P. Abbyad, X. Shi, S. G. Boxer, and C. R. Bagshaw, "Protonation, photobleaching, and photoactivation of yellow fluorescent protein (YFP 10C): a unifying mechanism," *Biochemistry* **44**, 5510–5524 (2005).
10. M. Zimmer, "Green fluorescent protein (GFP): applications, structure, and related photophysical behavior," *Chem. Rev. (Washington, D.C.)* **102**, 759–781 (2002).
11. A. Miyawaki and R. Y. Tsien, "Monitoring protein conformations and interactions by fluorescence resonance energy transfer between mutants of green fluorescent protein," *Methods Enzymol.* **327**, 472–500 (2000).
12. J. J. van Thor, T. Gensch, K. J. Hellingwerf, and L. N. Johnson, "Phototransformation of green fluorescent protein with UV and visible light leads to decarboxylation of glutamate 222," *Nat. Struct. Biol.* **9**, 37–41 (2002).